

pubs.acs.org/estair Article

On the Physicochemical Differences between Cloud Droplet Residual Particles and Below-Cloud Particles over the Northwest Atlantic

Published as part of ACS ES&T Air special issue "John H. Seinfeld Festschrift".

Grace Betito, Ewan C. Crosbie, Chris A. Hostetler, Simon Kirschler, Richard H. Moore, Taylor J. Shingler, Michael A. Shook, Leong Wai Siu, Christiane Voigt, Edward L. Winstead, Luke D. Ziemba, and Armin Sorooshian*



Cite This: https://doi.org/10.1021/acsestair.5c00150



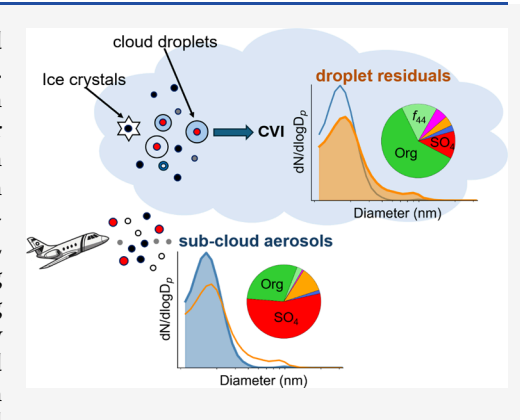
ACCESS

Metrics & More

Article Recommendations

s Supporting Information

ABSTRACT: Cloud droplet residual particles provide insight into cloud formation and processes controlling cloud radiative effects and precipitation. Aerosol particle size distribution and composition were measured in situ from an aircraft with a laser aerosol spectrometer (LAS) and an aerosol mass spectrometer (AMS), respectively, both of which switched between an isokinetic inlet when flying below cloud base (BCB) and a counterflow virtual impactor (CVI) when flying in cloud (above cloud base, ACB). Pairs of data linking below-cloud and incloud measurements reveal that the particle effective radius is up to a factor of 2 higher for in-cloud droplet residuals compared to below-cloud aerosol, suggesting some possible mix of preferential activation of larger particles, cloud processing that promoted larger droplet residuals, or other effects. Droplet residuals also show higher mass fractions of organics (and f_{44}) and chloride, with the latter correlated with factors suggestive of an increased sea salt influence. Case studies of African dust transported to Bermuda did not show a clear signature of the coarse aerosol



influence in droplet residual measurements, in contrast to sea salt cases. These results leverage a unique airborne data set from ACTIVATE over the northwest Atlantic, providing insight into preferential particle size and compositions describing the subset of particles serving as cloud condensation nuclei (CCN).

KEYWORDS: CVI, droplet residuals, size distribution, dust, sea salt, droplet activation, CCN

1. INTRODUCTION

Aerosols serve as cloud condensation nuclei (CCN), which are the seeds of cloud droplets. The physical and chemical characteristics of aerosols determine what fraction of them can serve as CCN at a given supersaturation, which is a central aspect of understanding aerosol-cloud interactions^{1,2} that are linked to the largest uncertainty in estimates of total anthropogenic radiative forcing.³ It is challenging to know exactly the properties of the special subset of particles that nucleate into cloud droplets since it requires capturing those droplets, drying them, and then subsequently characterizing those droplet residual particles. Moreover, these residuals carry a history beyond nucleation, which may involve further cloud processing effects, including, for instance, coalescence between droplets (i.e., two droplet residual particles merge into one) and chemical reactions in droplets that alter the original physicochemical properties of activated CCN.

Cloud droplet residuals are typically characterized with surface-based mountaintop measurements owing to the ease of intercepting clouds at high elevations e.g.,. 4–8 While surface-based measurements often reflect localized aerosol populations, they can also capture long-range transported and free tropospheric aerosols. 9,10 In addition, long-term ground-based observations provide important insights into seasonal trends in cloud droplet residual properties. 8,9,11 Airborne measurements complement these observations by allowing in situ sampling across varying altitudes, geographic locations, and meteorological regimes, offering a more comprehensive perspective. As noted by Zelenyuk et al., 12 aircraft measurements are best suited for CCN characterization due to the ease of comparing in-cloud CCN properties and below-cloud unactivated aerosol proper-

Received: April 27, 2025 Revised: August 28, 2025 Accepted: August 29, 2025



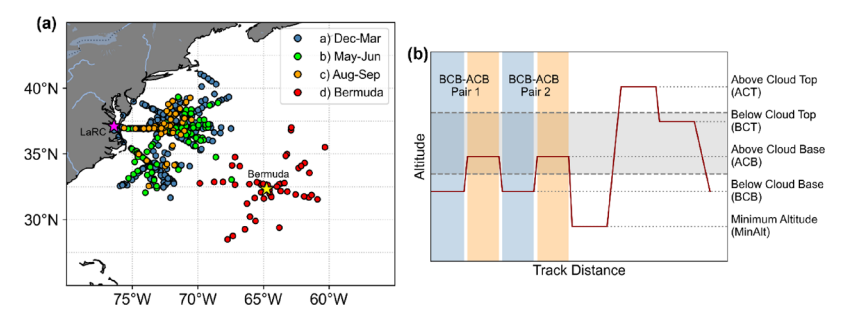


Figure 1. (a) Map of the sample region, where the circles represent the midpoints of BCB–ACB pairings colored by four categories. The stars indicate the locations of Bermuda and the main base of operations during ACTIVATE (NASA Langley Research Center in Hampton, Virginia). (b) Typical flight pattern of a cloud ensemble conducted by the HU-25 Falcon. In this study, we focus on two level legs: below cloud base (BCB) and above cloud base (ACB), denoted by blue and orange shading, respectively. The gray shading indicates the cloud layer.

ties. However, airborne studies of cloud droplet residuals have been conducted over short time periods in a fixed region, largely due to the complexity and cost associated with airborne sampling. Such campaigns have taken place in regions including northern Atlantic, ¹³ North Sea, ¹⁴ north-central Oklahoma, ¹⁸ most of the western United States, ¹⁶ southeastern Texas, ¹⁷ southeast Pacific Ocean, ¹⁸ Alaska, ^{12,19} and northeast Pacific Ocean. ^{20,21} This leaves critical gaps in understanding the spatial and seasonal variability of droplet residual properties, including over the northwest Atlantic where currently there is only one report regarding the composition of droplet residual properties with airborne measurements. ²²

Depending on the study region, the chemical composition of droplet residuals reveals key differences from subcloud aerosols. Sulfate and organics are typically the dominant components in both droplet residuals and below-cloud aerosols, with at least one study showing similar relative fractions of each both below and above cloud base over the northeast Pacific. 21 Some studies have shown that droplet residuals tend to have greater sulfate content compared to aerosols below and above clouds, 12,15 while others show enhanced organic content, 16 higher levels of oxygenated species among the organic fraction, 17,22 and increased fractions of both nitrate and organics.¹⁴ In addition, droplet residuals have been shown to contain significantly higher fraction of carbonates than ambient aerosols, along with increased levels of sea salt and black carbon. 19 A few past works have examined size distributions of droplet residuals, with examples being based on airborne measurements over the southeast Atlantic, 18 the North Sea between Rotterdam (Netherlands) to Newcastle (United Kingdom), 14 and the North Slope of Alaska, 12 in addition to surface based measurements at Mt. Åreskutan in Central Sweden,⁶ Puy de Dôme, France,²³ and at the mountain ridge Thüringer Wald in central Germany.^{24,25} These works showed that droplet residuals generally exhibit larger dry diameters than aerosols outside of clouds. Complementing these findings, seasonal variability in residual size was observed at the Zeppelin Observatory in the Arctic, with accumulation mode particles dominating in warmer months and Aitken mode particles more prevalent in colder months, indicating a seasonal shift in the size of activated particles.8

Here, we present findings from simultaneous aircraft-based measurements of the physical and chemical properties of ambient aerosol particles below cloud and cloud droplet residuals conducted during NASA's Aerosol Cloud meTeorology Interactions oVer the western ATlantic Experiment (ACTIVATE) campaign. Our key research questions are as

follows: (1) What are the dominant chemical and physical characteristics of ambient aerosols and cloud droplet residual particles over the northwestern Atlantic and how do they differ (if at all)? (2) How do these properties vary across different seasons and geographic locations? A unique aspect of this work as compared to those in the past is the very extensive statistical nature of the data set across multiple seasons and years and over a region offering very wide aerosol and cloud characteristics. Furthermore, the systematic and unique strategy of the ACTIVATE flights is very conducive to this study owing to the focus being placed on repeatedly alternating flight legs below and in the cloud.

2. METHODS

This section gives an overview of the instruments deployed during the 3-year ACTIVATE campaign and the data analyses used to determine and compare the size distribution and chemical characteristics of ambient aerosol and droplet residual particles. Although a brief summary is provided below, more detailed information on the campaign and instruments used can be found in Sorooshian et al.²⁹

2.1. Flight Campaign. ACTIVATE took place between 2020 and 2022 with a focus on aerosol-cloud-meteorology interactions.³⁰ Based mainly out of NASA's Langley Research Center with a small subset of flights based out of Bermuda (Figure 1a), ACTIVATE included six airborne measurement campaigns conducted during winter and summer each year.²⁹ Two spatially coordinated aircraft conducted systematic flight profiles in the form of "statistical surveys" comprised of both clear air and cloud ensemble measurements (hereafter "ensembles"), whereby a higher-flying King Air (~9 km altitude) conducted remote sensing measurements and launched dropsondes and a lower-flying HU-25 Falcon conducted in situ measurements of trace gases, aerosol particles, clouds/precipitation, and atmospheric state parameters in and just above the marine boundary layer (usually <3 km). In this study, we focus on the cloud ensembles performed whereby the Falcon conducted repeated sets of level legs (~3 min in duration or ~20 km in distance) in the following nominal order: below cloud base (BCB), above cloud base (ACB), a second pair of BCB and ACB, minimum altitude (MinAlt; ~150 m above sea level), above cloud top (ACT), and below cloud top (BCT) (Figure 1b). For this paper, we focus on BCB (subcloud-base aerosol particles) and ACB (cloud droplet residuals) pairs to compare their size and composition properties.

2.2. Instrumentation. Aerosol sampling on the Falcon alternated between an isokinetic inlet,³¹ which was used to

characterize aerosols below and above clouds, and a counterflow virtual impactor (CVI; Brechtel Manufacturing Inc.) inlet, which was employed to analyze cloud residual particles during cloud penetrations. A key consideration when interpreting the data collected behind the CVI is the inherent CVI sampling bias toward larger droplets above the cut size. Additionally, it is presumed that smaller droplets unable to pass the second stagnation plane and exit the tip could collide with larger droplets entering the probe, increasing the droplet size and producing larger residuals than an individual droplet alone. Two instruments sampled droplet residuals downstream of the CVI: a laser aerosol spectrometer (LAS) and an aerosol mass spectrometer (AMS). Both the LAS and AMS also sampled behind the isokinetic inlet. The LAS (TSI Inc. Model 3340) measured dry aerosol number size distribution for diameters between 100 and 3500 nm at 1 s time resolution. The instrument was calibrated using monodisperse ammonium sulfate particles with a refractive index of 1.52, which has been identified to broadly represent bulk ambient aerosol particles.³³ Regular spotchecks with NIST-traceable polystyrene latex spheres of appropriate sizes were conducted to verify the long-term stability in the LAS sizing performance. We caution that some of the LAS sizing characteristics beyond ~1000 nm are vulnerable to its nonmonotonic Mie response, and peaks at the larger sizes may therefore be artifacts. 34,35

A high-resolution time-of-flight aerosol mass spectrometer (AMS; Aerodyne)³⁶ measured nonrefractory chemical composition of dried ambient aerosol and droplet residuals including sulfate, nitrate, chloride, ammonium, and organics for the diameter range from 60 to 600 nm at a time resolution of 30 s, amounting to ~3.3 km horizontal resolution based on the Falcon's aircraft speed of \sim 110 m s⁻¹. We also utilize the mass spectral marker m/z 44 for oxygenated hydrocarbons, ³⁷ with f_{44} representing the ratio of m/z 44 to total organic mass. Due to its differencing method, AMS measurements can yield negative mass concentrations in clean conditions, which we retained in our statistical calculation to prevent biasing the leg-averaged values.²⁹ Note that for cloud droplet residuals, only speciated mass fractions from the AMS are reported. Mass concentration information from the AMS behind the CVI is not reported owing to appreciable uncertainties due to the nature of the CVI operation. Contextual information is used in the form of watersoluble ionic composition from a particle-into-liquid sampler (PILS; BMI) coupled to offline ion chromatography; ³⁸ note that the PILS was only operated downstream the isokinetic inlet. The PILS time resolution varies between 5 and 7 min (\sim 33–46 km), and the PILS data represent the diameter range of 50-5000 nm.²⁹

We also use 1 s data from the Fast Cloud Droplet Probe (FCDP; SPEC Inc.) for cloud screening purposes with reliance on both cloud droplet number concentration ($N_{\rm d}$) between 3 and 50 μ m and liquid water content (LWC). Additionally, we use Two-Dimensional Stereo probe (2D-S) data to calculate the ice mass fraction (IMF). For the pollution category classification, we use particle number concentrations of 0.003–5 μ m, measured by a condensation particle counter (CPC, TSI-3776).

For two case study flights, we also use data from the High Spectral Resolution Lidar – generation 2 (HSRL-2),⁴³ which was deployed on the King Air and is used here for vertically resolved information about aerosol types.⁴⁴ The aerosol types include urban, marine, polluted marine, fresh smoke, smoke, pure dust, and dusty mix. The HSRL-2 data are representative of

the column of the atmosphere below the King Air during flights, which were carefully coordinated with the Falcon such that the lidar profile measurements were coincident within 5 min in time and 6 km horizontal distance > 70% of the time. 45

2.3. Data Analysis. Because the Falcon requires time/distance to change the altitude, there is a horizontal gap between the BCB and ACB level flight legs. In this study, we select pairs of BCB and ACB legs, ensuring that the horizontal distance covered during the ACB leg did not exceed 40 km from the end of its corresponding BCB leg. The median distance between the nearest BCB and ACB legs for each season ranged from 15 to 19.5 km (Figure S1). To confirm cloud presence during ACB legs, we applied the following criteria: 40 LWC > 0.01 g m $^{-3}$ and $N_{\rm d}$ > 10 cm $^{-3}$. Cloud-free air in BCB legs was assumed to be present if LWC < 0.001 g m $^{-3}$ and $N_{\rm d}$ < 5 cm $^{-3}$. 46 Additionally, only BCB $^{-1}$ ACB pairs with a minimum in-cloud time of 10 s, 39 as well as availability of both LAS and AMS data for each pair, were included in the analysis. Table 1 summarizes the number of

Table 1. Median (25th—75th quartile) Values of Aerosol and Cloud Droplet Variables for Four Seasonal Categories during ACTIVATE^a

	$(cm^{-3})^a$	$\frac{\text{FCDP } N_{\text{d}}}{(\text{cm}^{-3})}$	LAS r _e (nm)		
			(>100 nm)	(≤1000 nm)	n
Dec-Mar ^b					
ВСВ	329 (229– 457)	0.2 (0.1- 0.3)	138 (109– 248)	119 (104– 142)	357
ACB	37 (19– 61)	293 (165– 489)	295 (190– 436)	198 (153– 248)	
May−Jun ^c					
BCB	258 (187- 401)	0.5 (0.2- 0.8)	271 (150- 452)	152 (126– 189)	116
ACB	45 (19– 61)	229 (126- 340)	274 (200– 362)	218 (179– 255)	
Aug-Sep ^b					
BCB	231 (148- 753)	0.4 (0.2- 0.6)	236 (135- 458)	135 (117– 167)	51
ACB	29 (14– 54)	171 (97– 256)	419 (248– 626)	242 (176– 290)	
Bermuda ^b					
ВСВ	257 (199– 326)	0.5 (0.3- 0.7)	273 (157- 472)	153 (127– 188)	45
ACB	16 (9–31)	142 (69- 255)	301 (218- 458)	252 (198– 300)	

"Data are separated based on two-level legs (BCB, ACB). Bermuda = flights based out of Bermuda in June 2022. The far right column shows the number of pairs per category. "Statistically significant difference in $r_{\rm e}$ for both the submicron-only (\leq 1000 nm) and the full LAS size range (>100 nm) between BCB and ACB legs based on the Mann—Whitney U test (p < 0.001). "Statistically significant difference in $r_{\rm e}$ for submicron-only.

selected BCB-ACB pairs throughout ACTIVATE deployments, amounting to 569 total pairs, with the winter season (December-March) deployments yielding the highest number of pairs (357 pairs).

We next applied an enhancement factor (EF) to the CVI data to correct for the enrichment of particles³² using the following equation:

$$EF = \frac{A_{tip}\nu_{plane}}{q_{sample}} \tag{1}$$

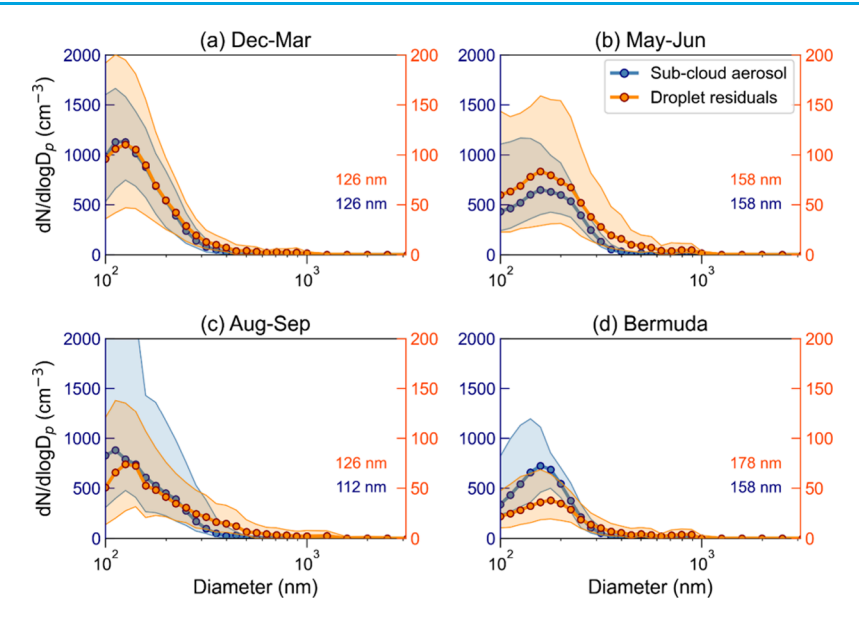


Figure 2. Dry particle number size distributions for (blue) subcloud aerosol sampled in BCB legs and (orange) cloud droplet residual particles sampled in ACB legs, with separate y-axes for (left, in blue) ambient aerosol and (right, in orange) droplet residual particles. Shaded areas represent the 25th—75th percentile range, while blue and orange numbers (in nm) show the modal diameter of aerosol particles and the droplet residuals, respectively.

where A_{tip} represents the area of the inlet tip where drops enter, v_{plane} denotes the aircraft's velocity, and q_{sample} is the volumetric flow rate of air sampled through the CVI inlet. The value of A_{tip} is 1.67×10^{-5} m², q_{sample} is 15 L min⁻¹, and the aircraft velocity ranges from 80 to 155 m s⁻¹. For the entire data set discussed here, the EF was in the range of 5-10.

We also calculate the dry effective radius (r_e) for both ambient and droplet residuals using LAS size distribution data, as described by the equation below:

$$r_e = \sum_{i=1}^{N} n_i r_i^3 / \sum_{i=1}^{N} n_i r_i^2$$
 (2)

where *N* is the number of bins, n_i is the number concentration (# cm⁻³) for individual size bins, and r_i is the bin-center radius.

ACTIVATE data are presented for four categories based on time of year and location of measurements: December–March, May–June, August–September, and "Bermuda", the latter being flights in June 2022 based from Bermuda. All other flights were based in Hampton, Virginia. The Bermuda flights were conducted to extend the spatial domain of the data set to farther eastward from the U.S. East Coast and Gulf Stream, where Hampton-based flights could not reach due to fuel limitations.

3. RESULTS AND DISCUSSION

3.1. Aerosol Particle and Droplet Residual Number Size Distributions. We first compare the aerosol number size distributions of below-cloud ambient aerosol and above-cloud base droplet residual particles for the four categories defined in Section 2.3 (Figure 2), with the number concentration statistics shown in Table 1. We do not focus on above-cloud aerosols as the predominant aerosol activating into droplets stem from the BCB legs.³⁹ We caution that this analysis cannot discriminate residuals that are dried versions of the particles that activated into cloud droplets from residuals of particles that have undergone modification due to cloud processing. The data discussed herein likely reflect a combination of both types of particles.

Both subcloud aerosol and droplet residual particles showed similar unimodal number size distributions across the four categories (Figure 2). Modal diameters for subcloud particles and droplet residuals range from 112 to 158 nm and 126 to 178 nm, respectively, with median aerosol number concentrations for subcloud aerosols ranging from 231 to 329 cm⁻³ and for droplet residuals from 16 to 45 cm⁻³. The highest median aerosol number concentration (N_a) for BCB legs, as well as N_d for ACB legs, were observed in December-March (Table 1). For context, the median droplet number concentrations measured by the FCDP during the times of CVI-LAS measurements ranged from 142 to 293 cm⁻³ and thus exceeded the droplet residual concentrations, which is a helpful sanity check as $N_{\rm d}$ includes more activated particles below the lowest diameter of the LAS (100 nm) and due to the innate nature of CVI sampling that is vulnerable to particle losses and transmission efficiency dependency on droplet size.³² Past work for ACTIVATE demonstrates that there can be activation of particles below 100 nm. 47,48

Droplet residual particles exhibited slightly larger modal diameters than subcloud particles for the August-September (126 versus 112 nm) and Bermuda (178 versus 158 nm) categories. A possible reason for the shift to larger sizes in droplet residuals could be the preferential activation of larger particles and/or cloud processing that promoted larger droplet residual particles via some combination of aqueous chemistry to generate new mass and collision-coalescence of drops to increase the size of the droplet residuals. 49,50 Although based on only 2022 ACTIVATE data, which had the most flights, Edwards et al. 51 showed that sea salt levels were highest based on Falcon measurements with the PILS in the Bermuda category, consistent with a higher modal diameter for droplet residual particles in that season. Liu et al.⁵² showed for 2020 ACTIVATE deployments that the August-September time frame exhibited higher sea salt aerosol levels than the winter period of February-

For comparison, other studies also reported that modal diameters of cloud droplet residuals are generally larger than ambient aerosol particles. ^{6,12} Zelenyuk et al. ¹² reported that

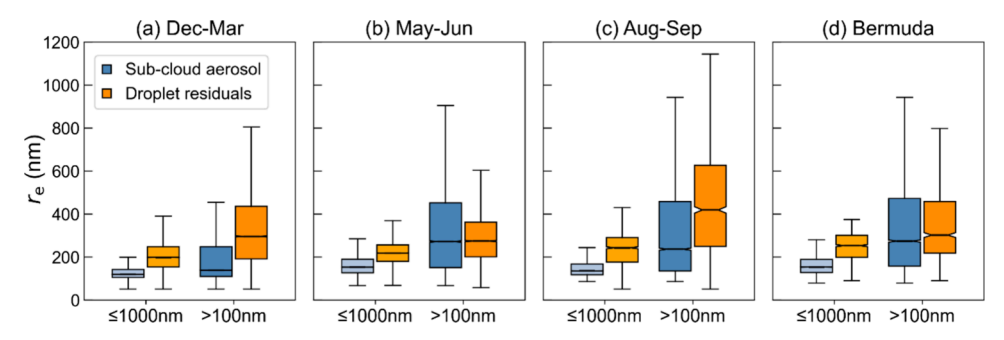


Figure 3. Box notch plots comparing effective radius (r_e) for (blue) subcloud particles and (orange) cloud droplet residual particles for submicron-only (\leq 1000 nm) and including supermicron (>100 nm). The median is represented by the horizontal line within each box with the box edges marking the 25th and 75th percentiles. The whiskers extend to the upper boundary (third quartile +1.5 × interquartile range) and the lower boundary (first quartile -1.5 × interquartile range). Notches around the median denote its 95% confidence interval.

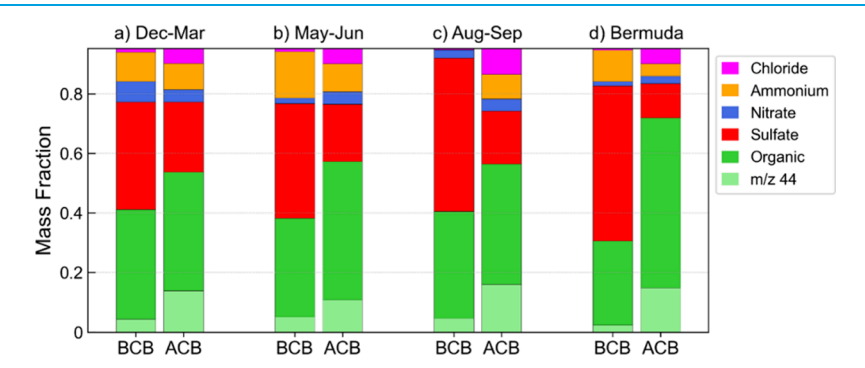


Figure 4. Seasonal comparison of AMS mass fractions for subcloud aerosol (BCB legs) and droplet residual particles (ACB legs). Parts of the Organic bars are shaded light green to represent the relative fraction of organics comprised of oxygenated organic species represented by the m/z 44 marker.

particles below cloud show peak abundance at 227 nm, while cloud residuals peak at 265 nm at the North Slope of Alaska. Although Graham et al.⁶ did not provide the exact values, their plot indicates that the modal diameter of particles before cloud events is approximately 70 nm, compared to around 140 nm for cloud residuals on Mt. Åreskutan in Central Sweden.

We also examined the subcloud and droplet residual number size distributions, binned by temperature, to assess whether there was a change in modal size with respect to temperature (Figure S2). In general, the modal size decreased with decreasing temperature, except during December-March when it increased for temperature bins colder than -10 °C. Using available 2D-S and FCDP measurements, we calculated IMF⁴¹ and verified that the clouds sampled during ACB legs included in this study were predominantly in the liquid phase. Thus, the reversal in modal size is unlikely to be due to ice-phase processes and may instead reflect reduced activation of smaller particles under lower supersaturation conditions.² Similarly, we classified our BCB-ACB pairings into different pollution categories based on subcloud condensation nuclei (CN) concentration: clean: <300 cm⁻³; intermediately polluted: 300-900 cm⁻³, and polluted: 900-1600 cm⁻³ (Figure S3). 53,54 This categorization allows us to examine whether pollution levels influence residual particles sizes. We found no substantial difference in modal diameter between the clean and intermediate categories, suggesting that increases in aerosol number concentration within these ranges do not significantly impact droplet residual size. However, for the polluted category, the number size distributions shift toward a smaller size range (except in May-June), likely due to increased competition for water vapor among the larger number of activated particles. This trend is consistent with the temperature-binned results, where

droplet residual sizes tended to be smaller at colder temperatures, potentially reflecting suppressed condensational growth. Our findings contrast with observations from a study off the California coast, which reported minimal differences in residual particle size distribution across varying pollution levels, with most variability attributed to number concentrations rather than mode or volume. ⁵⁴

Owing to the minimum size measured by the LAS, this instrument cannot capture the Hoppel minimum, ⁵⁵ which typically exists at smaller sizes (60–100 nm) for the ACTIVATE data set based on recent studies. ^{39,56,57} The Hoppel minimum, a gap in the size distribution separating two distinct modes, typically represents the smallest particles capable of serving as CCN under specific thermodynamic conditions influenced by cloud processing. ⁵⁵ Cloud residuals can exist in sizes smaller than the Hoppel minimum, as reported in studies conducted in the central Arctic Ocean ⁵⁸ and at Puy de Dôme, France. ²³

Next, we calculate the $r_{\rm e}$ for both submicron-only particles ($\leq 1000~\rm nm$) and for the full size range including supermicron particles (>100 nm), comparing subcloud aerosols and droplet residual particles. While the submicron-only data more clearly highlight the differences, both approaches consistently show that droplet residuals generally have larger $r_{\rm e}$ than subcloud aerosols (Figure 3). The differences in $r_{\rm e}$ are statistically significant (p-value = <0.001) for all seasons for the submicron-only range and for the full size range except during May–June. Median $r_{\rm e}$ for droplet residual particles were, on average, larger than those for subcloud aerosol, particularly during December–March and August–September for both the submicrometer-only and full size ranges. Figure S4 shows seasonal histograms of $r_{\rm e}$ differences (ACB–BCB) for particles >100 and $\leq 1000~\rm nm$, with inset boxplots showing corresponding ACB/BCB $r_{\rm e}$ ratios.

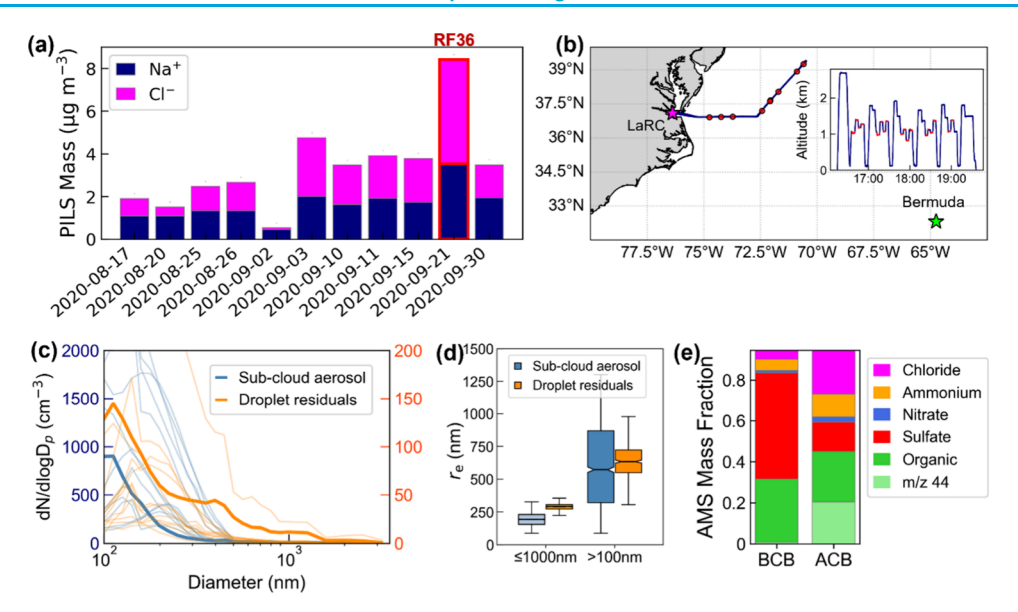


Figure 5. (a) Average mass concentration of PILS Na⁺ and Cl⁻ for August–September for BCB leg. The stacked bar with a red edge (RF36: 21 September 2020) marks the flight date used for the sea salt case study. Shown also are (b) the Falcon flight path, with circles indicating the locations of BCB–ACB pairings, (c) LAS number size distributions for subcloud particles in BCB legs and droplet residuals in ACB legs, with thick lines representing the median for RF36, and thin lines representing the median for other flights in the August–September category, (d) calculated effective radius (r_e) for submicron-only (\leq 1000 nm) and including supermicron (>100 nm), and (e) average mass fraction of speciated mass from AMS including the relative contribution of m/z 44 to total organic mass.

Differences are mostly positive, indicating a larger $r_{\rm e}$ in droplet residuals. Seasonal variability is evident, with broader, positively skewed distributions and higher ratios during December—March, while differences are near zero and ratios are close to unity during May—June, indicating minimal differences. Selected pairs where BCB has a larger $r_{\rm e}$ than ACB are explored further in Section 3.3.2.

3.2. Chemical Properties of Aerosol Particles and **Cloud Droplet Residuals.** This section compares the chemical compositions of ambient aerosols (BCB leg) and droplet residual particles (ACB leg) using CVI-AMS data. The analysis builds on a previous study,²² which examined chemical composition data from 2020 to 2021 across various flight legs. The distinction in this analysis is both a larger data set as almost half of the ACTIVATE flights were in 2022 and the inclusion of data around Bermuda, which extends the data set into a more remote marine region. The results of the larger data set and inclusion of Bermuda data are still consistent with Dadashazar et al., 22 in that droplet residual particles were richer in organic material and had less sulfate compared to subcloud ambient aerosol (Figure 4). The difference between BCB and ACB data is most distinct for the Bermuda data set. Compared with other studies, AMS measurements of droplet residuals from warm tropospheric clouds at a ground site on Mt. Åreskutan revealed that organic and nitrate-containing particles were more readily activated into cloud droplets than sulfate.⁵ Additionally, increased fractions of organics and nitrate in droplet residuals have been observed in the North Sea.¹⁴ Their findings also suggest that larger aerosol particles were preferentially incorporated into the droplets. Another study over the northeast Pacific reported similar relative fractions of organics and sulfate both below and above cloud base.²¹

For a more detailed look at individual BCB–ACB pairs, we computed the organic:sulfate ratio using the mass fraction of both species and plotted the ratios for subcloud aerosols (*x*-axis) and droplet residuals (*y*-axis) for each season (Figure S5). Points

below the 1:1 line indicate that the organic:sulfate ratio is lower in droplet residuals compared to subcloud aerosols. Overall, the ratio is higher in droplet residuals compared to subcloud aerosols, with only 16% of the total points below the 1:1 line.

The combined LAS and AMS results show that droplet residuals carry a physicochemical signature of being larger and more organic-rich than subcloud particles, and that those organics are more functionalized such as what has been shown in past studies linked cloud chemistry to production of dicarboxylic acids like oxalate. 59-61 These differences are pronounced, especially for composition, for the Bermuda data set, which is unexpected as this area is farthest removed from continental emissions that would presumably lead to secondary organic aerosol during cloud processing. One possible explanation could be due to the type of cloud system encountered during Bermuda flights. Much of the cloud water samples from Bermuda were collected during process study flights, which probed deeper cumulus clouds as detailed by Crosbie et al. 48 The flight strategy of the Falcon in ACTIVATE's process study flights involved stacked level legs ranging from below to above clouds, and thus, there is a more defined bias for ACB measurements to represent a processed state compared to the BCB precursor state. During the statistical survey flights closer to the U.S. East Coast, the BCB-ACB leg pairs do not reflect as clear of a temporal progression, as the air parcels may have circulated through clouds multiple times before being sampled at the BCB. This is speculative and opens an opportunity for future analysis to examine how different cloud types and flight strategies impact differences between BCB particles and ACB droplet residuals.

In summary, in addition to the observed compositional shift toward more organic and oxygenated materials in droplet residuals, our findings further support the possibility of size modification through cloud processing, as indicated by the larger size of residual particles compared to subcloud aerosols. Understanding the chemical composition of individual cloud droplets is a powerful approach to advancing knowledge of

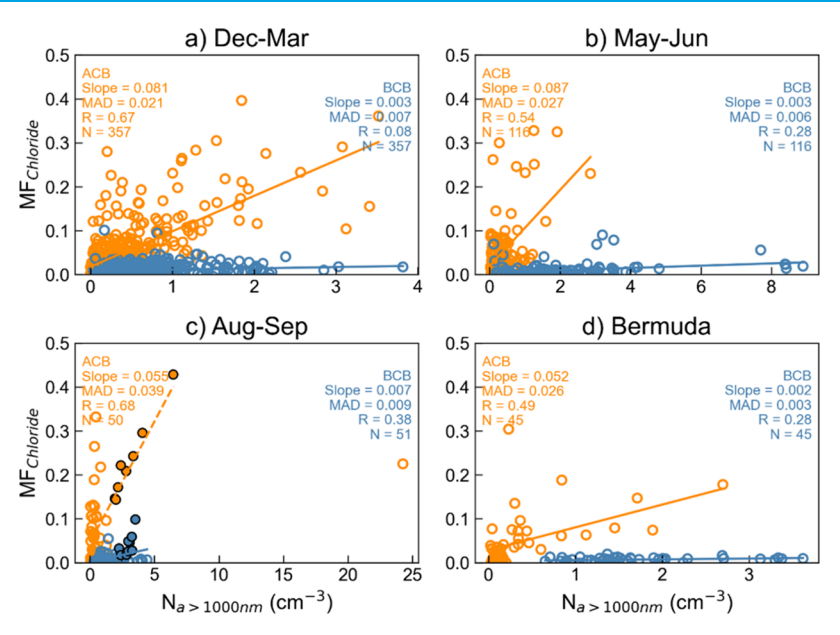


Figure 6. Scatterplot of AMS chloride mass fraction versus LAS number particles above 1000 nm ($N_{\text{a>1000 nm}}$). The circles with solid colors correspond to BCB–ACB pairs used for the sea salt case study in Figure 5. MAD is mean absolute deviation.

aerosol-cloud interactions and improving parametrizations of cloud microphysics and aerosol scavenging processes. Continued in situ observational studies are necessary for refining microphysical models and enhancing accuracy of such parametrizations. In particular, information on the droplet residual composition is essential for evaluating whether models such as Weather Research and Forecasting model coupled with chemistry (WRF-Chem) can accurately reproduce observed trends in droplet residual chemical fractions. Such insights also enable better representation of aerosol-cloud interactions by accounting for the aerosol chemical composition and spatiotemporal variability of the aerosols that actually serve as CCN.

3.3. Case Studies. The case study flights presented below were identified based on flight scientist notes documented in Sorooshian et al.²⁹

3.3.1. High Sea Salt Loading. We explore a high sea salt case flight from 21 September 2020, (RF36) to determine whether differences in aerosol size are observed (Figure 5). The elevated sea salt loading during this flight was likely due in part to very high wind speeds, as noted in the flight scientist's notes.²⁹ For this case study, nine BCB-ACB pairs passed the data filtering criteria (Section 2.3). We leveraged PILS sodium and chloride measurements to quantify sea salt concentration for this flight, which was a typical out-and-back flight from Hampton, Virginia to the northeast. The chloride mass concentration from PILS measurements for BCB leg ranged from 2.6 to 6.3 μ g m⁻³ (mass fractions of 0.43 to 0.44), which is elevated compared to the rest of the flights during this season (0.4–2.8 μ g m⁻³, mass fractions of 0.03 to 0.42). Similarly, sodium mass concentration ranged from 2.2 to 4.3 μ g m⁻³ (mass fractions of 0.36 to 0.39), placing it on the higher end relative to other flights in this season (0.45-1.9 μ g m⁻³, mass fractions of 0.19 to 0.40).

While AMS cannot robustly measure refractory chemical composition including sea salt sodium, previous studies have shown that it can detect signals from certain sea salt components, including NaCl, chloride, and iodide. $^{22,68-73}$ Based on this, we examined the mass fraction of chloride (MF_{chloride}) from the AMS to assess the potential enhancement

during this flight. The median $MF_{chloride}$ values for droplet residuals and subcloud aerosols were 0.21 and 0.03, respectively, both higher than their respective seasonal median values of 0.07 and 0.007.

The number concentration of supermicron particles $(N_{\rm a>1000~nm})$ in cloud residuals during the 9 ACB legs $(2.1-6.5~{\rm cm}^{-3})$ was elevated compared to other flights (except on 26 August 2020, when the highest $N_{\rm a>1000~nm}$ of 24.3 cm⁻³ was observed). This is also evident in the number size distributions (Figure 5c). For BCB legs, $N_{\rm a>1000~nm}$ ranged from 2.2 to 3.5 cm⁻³, also exceeding the seasonal median $(1.4~{\rm cm}^{-3})$. The calculated median $r_{\rm e}$ for the full size range (and submicron-only) were 572 nm (193 nm) and 633 nm (292 nm) for BCB and ACB legs, respectively, both higher than the seasonal median values for August—September, which were 236 nm (135 nm) and 419 nm (242 nm) for BCB and ACB, respectively (Table 1).

This case study provides evidence for the sea salt particle influence in droplet residual particles from both the number size distribution and composition perspectives. Sea salt particles would be expected to increase r_e , $N_{a>1000 \text{ nm}}$, and MF_{chloride} based on both general expectations and results in Figure 5. Figure 6 shows more broadly for the full ACTIVATE data set the relationship between $\mathrm{MF}_{\mathrm{chloride}}$ and $N_{\mathrm{a>1000~nm}}$, showing a positive relationship for droplet residual measurements in all four categories albeit with a wide range of correlation coefficients (r: 0.49–0.68) and innate noise around the best fit lines. BCB legs show flatter relationships (slopes ≤ 0.007 in contrast to 0.05-0.08 for ACB) and a wider range of correlations (r: 0.08–0.38). Figure S6 is consistent in that there are positive relationships between $N_{
m a>1000~nm}$ and $r_{
m e}$ but with stronger correlations for both ACB and BCB measurements. Thus, these data generally support the notion that coarse sea salt particles are influencing droplet residual properties and integral to aerosol-cloud interactions in the study region. Based on model results, several studies 74,75 have shown that sea salt can influence cloud droplet activation by either suppressing or enhancing it, depending on environmental conditions. Under high sulfate aerosol concentrations and weak updrafts, sea salt may suppress activation by competing for water vapor, while

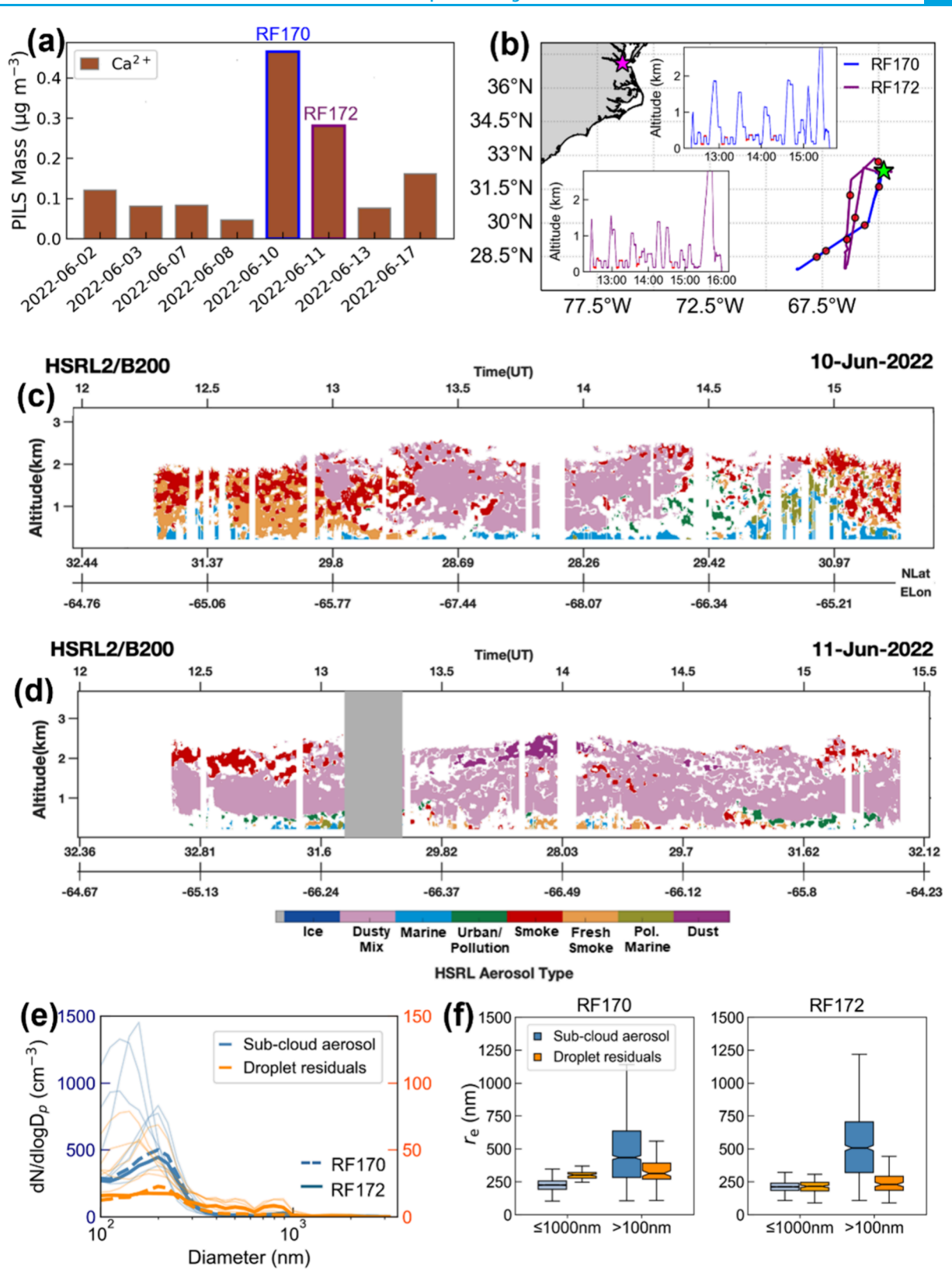


Figure 7. (a) Average mass concentration of PILS Ca^{2+} for the Bermuda category during BCB legs of different flights. The stacked bars with the blue edge (RF170: 10 June 2022) and purple edge (RF172: 11 June 2022) indicate the flight dates used for the dust influence case studies. Also shown are the (b) flight path, with circles indicating the locations of BCB−ACB pairings, (c−d) HSRL-2 aerosol type vertical distribution, (e) LAS number size distributions for subcloud particles in BCB legs and droplet residuals in ACB legs, and (f) calculated effective radius (r_e) for submicron-only (≤1000 nm) and supermicron (>100 nm). The thicker broken line in (e) represents the median for RF170, the thicker solid line represents the median for RF172, and thin lines represent median distributions for other flights based out of Bermuda in June 2022.

under low sulfate conditions and strong updrafts, it can enhance droplet formation. This mechanism in which sea salt indirectly influences sulfate activation, can affect marine boundary cloud albedo and, ultimately, can influence cloud lifetime and precipitation processes. ^{74,75}

3.3.2. African Dust Influence. Next, we examine two flights (RF170: 10 June 2022, and RF172: 11 June 2022) performed in Bermuda that were influenced by Saharan dust, as indicated by airmass trajectory analysis already shown elsewhere. ^{48,57} Four BCB–ACB pairs from RF170 and four from RF172 passed the filtering criteria for these flights.

For 10 June 2020 (RF170), the PILS Ca^{2+} mean (median) mass concentration is 0.47 (0.47) μ g m⁻³, while for 11 June 2022 (RF172), the mean (median) is 0.28 (0.16) μ g m⁻³, both higher compared to the other Bermuda flights (mean = 0.09, median = 0.06 μ g m⁻³). The HSRL aerosol classification scheme for RF170 showed more diverse aerosol types at the start of the flight, suggesting more complex source contributions, with a transition to a more dusty mix signature in the middle of the flight (Figure 7c). Siu et al. ⁷⁶ also examined this flight and reported a high depolarization ratio suggestive of the African dust influence. The flight on the next day (RF172) showed a more consistent dusty mix layer between the 0.5–2 km altitude, indicative of long-range transported dust with less mixing (Figure 7d).

The number of particles above 1000 nm $(N_{a>1000 \text{ nm}})$ for RF170 and RF172 had a median of 3 cm⁻³, which is elevated compared to the median value for other flights in this category (1.4 cm^{-3}) . Correspondingly, the r_e values for these cases for the full size range were consistently higher in subcloud aerosols than in droplet residuals but lower for the submicron-only range (Figure 7f). Unlike the sea salt case study, an increase in particle size in droplet residuals was not observed, likely reflecting the lower hygroscopicity of dust particles even after its long-range transport over the Atlantic as noted by others, too.7 Presumably, supermicrometer particles like dust particles act as CCN due to their larger size even with lower hygroscopicity. Dust can also become more CCN-active through internal mixing with soluble species like sulfate and nitrate from anthropogenic sources^{79,80} or via cloud processing.^{81,82} However, we cannot assess the extent to which the dust plume in our study experienced such processing. The lack of observed enhancement in the size of droplet residuals may just be due to the low concentration in the ACB leg. For example, Edwards et al.⁸³ analyzed the influence of African dust on CCN concentration reaching coastal southeast Florida and observed a lack of increase in CCN concentration due to the low number concentration of these presumably larger particles. Since our data set lacks direct measurements of dust-related chemical species and particle size distribution in the larger size range in droplet residuals, further investigation is needed.

4. OUTCOMES AND LIMITATIONS

Our results indicate that droplet residuals are larger in size than subcloud aerosols and exhibit higher mass fractions of organics (that are more oxygenated) and chloride. A case study under high sea salt loading showed enhancements in both effective radius and mass fraction of chloride in both subcloud and droplet residuals. In contrast, the transported African dust case did not show a corresponding increase in the particle size within droplet residuals. Both the temperature- and pollution-binned analyses reveal that the modal diameter of droplet residuals tends to decrease either with decreasing temperature or

increasing aerosol number concentration, indicating that environmental conditions such as colder temperatures or enhanced competition for water vapor can shift the residual size distribution toward smaller modes.

This study builds on prior work on cloud droplet chemistry by analyzing droplet residual number size distributions that have remained less explored in this region. While our results are not unexpected, they are valuable, given the limited observational data available in the region. Understanding the chemical and microphysical properties of cloud droplet residuals is essential for improving aerosol-cloud interaction parametrizations and refining cloud microphysical models. One important limitation of this study is that the subcloud aerosols (BCB leg) and cloud droplet residuals (ACB leg) were not measured simultaneously, and with the exception of some process study flights like in Bermuda, the BCB-ACB leg pairs were not vertically stacked but rather conducted in stair step fashion. Additionally, the absence of interstitial aerosol measurements limits our ability to quantify the scavenging efficiency. Also, due to constraints with CVI operation relating to flow rates and desired time resolution of in-cloud data, complementary instrumentation such as the SMPS and PILS could not be integrated, limiting our ability to more fully characterize the aerosol size distribution (to below 100 nm) and composition (e.g., sea salt, dust tracer species). While the number of flights during the Bermuda deployment was smaller compared to other seasons, the data set remains statistically robust, especially when compared with other airborne campaign studies. Moving forward, we recommend that future research efforts expand sampling to other geographic regions and find creative solutions to add more comprehensive measurements downstream of CVI inlets.

ASSOCIATED CONTENT

Data Availability Statement

The ACTIVATE data set is available at 10.5067/SUBORBITAL/ACTIVATE/DATA001.

Supporting Information

The Supporting Information is available free of charge at https://pubs.acs.org/doi/10.1021/acsestair.5c00150.

Figures for the median horizontal distance between ACB and BCB leg measurements; dry particle number size distribution binned by leg-mean temperature; dry particle number size distribution by pollution category; histogram and boxplots of effective radius differences between ACB and BCB legs; scatterplot of organic:sulfate mass fraction ratios for subcloud aerosols and droplet residuals; and scatterplot of effective radius versus $N_{\rm a>1000~nm}$ (PDF)

AUTHOR INFORMATION

Corresponding Author

Armin Sorooshian — Department of Hydrology and Atmospheric Sciences and Department of Chemical and Environmental Engineering, University of Arizona, Tucson, Arizona 85721, United States; Occid.org/0000-0002-2243-2264; Email: armin@arizona.edu

Authors

ı

Grace Betito − Department of Hydrology and Atmospheric Sciences, University of Arizona, Tucson, Arizona 85721, United States; ⑤ orcid.org/0000-0003-1332-658X

- Ewan C. Crosbie NASA Langley Research Center, Hampton, Virginia 23681, United States; Analytical Mechanics Associates, Inc., Hampton, Virginia 23666, United States
- Chris A. Hostetler NASA Langley Research Center, Hampton, Virginia 23681, United States
- Simon Kirschler Institute of Atmospheric Physics, German Aerospace Center, Cologne 82234, Germany; Institute of Atmospheric Physics, Johannes Gutenburg University Mainz, Mainz 55128, Germany
- Richard H. Moore NASA Langley Research Center, Hampton, Virginia 23681, United States; ⊚ orcid.org/0000-0003-2911-4469
- Taylor J. Shingler NASA Langley Research Center, Hampton, Virginia 23681, United States; ⊚ orcid.org/0000-0003-4596-1027
- Michael A. Shook NASA Langley Research Center, Hampton, Virginia 23681, United States
- Leong Wai Siu Department of Hydrology and Atmospheric Sciences, University of Arizona, Tucson, Arizona 85721, United States; Occid.org/0000-0002-1271-8445
- Christiane Voigt Institute of Atmospheric Physics, German Aerospace Center, Cologne 82234, Germany; Institute of Atmospheric Physics, Johannes Gutenburg University Mainz, Mainz 55128, Germany
- Edward L. Winstead NASA Langley Research Center, Hampton, Virginia 23681, United States
- Luke D. Ziemba NASA Langley Research Center, Hampton, Virginia 23681, United States

Complete contact information is available at: https://pubs.acs.org/10.1021/acsestair.5c00150

Notes

The authors declare no competing financial interest.

ACKNOWLEDGMENTS

ACTIVATE data analysis was funded by NASA grant 80NSSC19K0442 in support of the ACTIVATE Earth Venture Suborbital-3 (EVS-3) investigation, which is funded by NASA's Earth Science Division and managed through the Earth System Science Pathfinder Program Office. U-AZ funding also comes from ONR grant no. N00014-21-1-2115. C.V. and S.K. acknowledge funding by DFG within project no. 522359172 (SPP HALO 1294) and by the European Union's Horizon Europe program under grant no. 101192301 (A4CLIMATE). The authors gratefully acknowledge the pilots and aircraft maintenance personnel of the NASA Langley Research Services Directorate for conducting ACTIVATE flights, and all individuals who contributed to the successful implementation of the ACTIVATE campaign.

REFERENCES

- (1) Andreae, M. O.; Rosenfeld, D. Aerosol-cloud-precipitation interactions. Part 1. The nature and sources of cloud-active aerosols. *Earth-Sci. Rev.* **2008**, *89* (1–2), 13–41.
- (2) Dusek, U.; Frank, G. P.; Hildebrandt, L.; Curtius, J.; Schneider, J.; Walter, S.; Chand, D.; Drewnick, F.; Hings, S.; Jung, D.; et al. Size Matters More Than Chemistry for Cloud-Nucleating Ability of Aerosol Particles. *Science* **2006**, *312*, 1375–1378.
- (3) Bellouin, N.; Quaas, J.; Gryspeerdt, E.; Kinne, S.; Stier, P.; Watson-Parris, D.; Boucher, O.; Carslaw, K. S.; Christensen, M.; Daniau, A. L.; et al. Bounding Global Aerosol Radiative Forcing of Climate Change. *Rev. Geophys.* **2020**, *58* (1), No. e2019RG000660.

- (4) Adachi, K.; Tobo, Y.; Koike, M.; Freitas, G.; Zieger, P.; Krejci, R. Composition and mixing state of Arctic aerosol and cloud residual particles from long-term single-particle observations at Zeppelin Observatory. *Svalbard. Atmos. Chem. Phys.* **2022**, 22 (21), 14421–14439.
- (5) Drewnick, F.; Schneider, J.; Hings, S. S.; Hock, N.; Noone, K.; Targino, A.; Weimer, S.; Borrmann, S. Measurement of Ambient, Interstitial, and Residual Aerosol Particles on a Mountaintop Site in Central Sweden using an Aerosol Mass Spectrometer and a CVI. *J. Atmos. Chem.* **2006**, 56 (1), 1–20.
- (6) Graham, E. L.; Zieger, P.; Mohr, C.; Wideqvist, U.; Hennig, T.; Ekman, A. M. L.; Krejci, R.; Ström, J.; Riipinen, I. Physical and chemical properties of aerosol particles and cloud residuals on Mt. Areskutan in Central Sweden during summer 2014. *Tellus B* 2020, 72 (1), 1–16.
- (7) Gramlich, Y.; Siegel, K.; Haslett, S. L.; Freitas, G.; Krejci, R.; Zieger, P.; Mohr, C. Revealing the chemical characteristics of Arctic low-level cloud residuals in situ observations from a mountain site. *Atmos. Chem. Phys.* **2023**, 23 (12), 6813—6834.
- (8) Karlsson, L.; Krejci, R.; Koike, M.; Ebell, K.; Zieger, P. A long-term study of cloud residuals from low-level Arctic clouds. *Atmos. Chem. Phys.* **2021**, 21 (11), 8933–8959.
- (9) Zieger, P.; Heslin-Rees, D.; Karlsson, L.; Koike, M.; Modini, R.; Krejci, R. Black carbon scavenging by low-level Arctic clouds. *Nat. Commun.* **2023**, *14* (1), 5488.
- (10) Cozic, J.; Verheggen, B.; Mertes, S.; Connolly, P.; Bower, K.; Petzold, A.; Baltensperger, U.; Weingartner, E. Scavenging of black carbon in mixed phase clouds at the high alpine site Jungfraujoch. *Atmos. Chem. Phys.* **2007**, *7*, 1797–1807.
- (11) Pereira Freitas, G.; Kopec, B.; Adachi, K.; Krejci, R.; Heslin-Rees, D.; Yttri, K. E.; Hubbard, A.; Welker, J. M.; Zieger, P. Contribution of fluorescent primary biological aerosol particles to low-level Arctic cloud residuals. *Atmos. Chem. Phys.* **2024**, 24 (9), 5479–5494.
- (12) Zelenyuk, A.; Imre, D.; Earle, M.; Easter, R.; Korolev, A.; Leaitch, R.; Liu, P.; Macdonald, A. M.; Ovchinnikov, M.; Strapp, W. In Situ Characterization of Cloud Condensation Nuclei, Interstitial, and Background Particles Using the Single Particle Mass Spectrometer, SPLAT II†. *Anal. Chem.* **2010**, *82*, 7943–7951.
- (13) Glantz, P.; Noone, K. J.; Osborne, S. R. Comparisons of Airborne CVI and FSSP Measurements of Cloud Droplet Number Concentrations in Marine Stratocumulus Clouds. *J. Atmos. Ocean. Technol.* **2003**, *20*, 133–142.
- (14) Crumeyrolle, S.; Weigel, R.; Sellegri, K.; Roberts, G.; Gomes, L.; Stohl, A.; Laj, P.; Momboisse, G.; Bourianne, T.; Puygrenier, V.; et al. Airborne investigation of the aerosols—cloud interactions in the vicinity and within a marine stratocumulus over the North Sea during EUCAARI (2008). *Atmos. Environ.* **2013**, *81*, 288–303.
- (15) Saliba, G.; Bell, D. M.; Suski, K. J.; Fast, J. D.; Imre, D.; Kulkarni, G.; Mei, F.; Mülmenstädt, J. H.; Pekour, M.; Shilling, J. E.; et al. Aircraft measurements of single particle size and composition reveal aerosol size and mixing state dictate their activation into cloud droplets. *Environ. Sci. Atmos.* **2023**, *3* (9), 1352–1364.
- (16) Twohy, C. H.; Toohey, D. W.; Levin, E. J. T.; DeMott, P. J.; Rainwater, B.; Garofalo, L. A.; Pothier, M. A.; Farmer, D. K.; Kreidenweis, S. M.; Pokhrel, R. P.; et al. Biomass Burning Smoke and Its Influence on Clouds Over the Western U. S. *Geophys. Res. Lett.* **2021**, 48 (15), No. e2021GL094224.
- (17) Sorooshian, A.; Lu, M.-L.; Brechtel, F. J.; Jonsson, H.; Feingold, G.; Flagan, R. C.; Seinfeld, J. H. On the Source of Organic Acid Aerosol Layers above Clouds. *Environ. Sci. Technol.* **2007**, *41*, 4647–4654.
- (18) Twohy, C. H.; Anderson, J. R.; Toohey, D. W.; Andrejczuk, M.; Adams, A.; Lytle, M.; George, R. C.; Wood, R.; Saide, P.; Spak, S.; et al. Impacts of aerosol particles on the microphysical and radiative properties of stratocumulus clouds over the southeast Pacific Ocean. *Atmos. Chem. Phys.* **2013**, *13* (5), 2541–2562.
- (19) Hiranuma, N.; Brooks, S. D.; Moffet, R. C.; Glen, A.; Laskin, A.; Gilles, M. K.; Liu, P.; Macdonald, A. M.; Strapp, J. W.; McFarquhar, G. M. Chemical characterization of individual particles and residuals of cloud droplets and ice crystals collected on board research aircraft in the ISDAC 2008 study. *J. Geophys. Res. Atmos.* **2013**, *118* (12), 6564–6579.

- (20) Sorooshian, A.; MacDonald, A. B.; Dadashazar, H.; Bates, K. H.; Coggon, M. M.; Craven, J. S.; Crosbie, E.; Hersey, S. P.; Hodas, N.; Lin, J. J.; et al. A multi-year data set on aerosol-cloud-precipitation-meteorology interactions for marine stratocumulus clouds. *Sci. Data* **2018**, *5*, No. 180026.
- (21) Coggon, M. M.; Sorooshian, A.; Wang, Z.; Metcalf, A. R.; Frossard, A. A.; Lin, J. J.; Craven, J. S.; Nenes, A.; Jonsson, H. H.; Russell, L. M.; et al. Ship impacts on the marine atmosphere: insights into the contribution of shipping emissions to the properties of marine aerosol and clouds. *Atmos. Chem. Phys.* **2012**, *12* (18), 8439–8458.
- (22) Dadashazar, H.; Corral, A. F.; Crosbie, E.; Dmitrovic, S.; Kirschler, S.; McCauley, K.; Moore, R.; Robinson, C.; Schlosser, J. S.; Shook, M.; et al. Organic enrichment in droplet residual particles relative to out of cloud over the northwestern Atlantic: analysis of airborne ACTIVATE data. *Atmos. Chem. Phys.* **2022**, *22* (20), 13897–13913
- (23) Schwarzenboeck, A.; Heintzenberg, J.; Mertes, S. Incorporation of aerosol particles between 25 and 850 nm into cloud elements measurements with a new complementary sampling system. *Atmos. Res.* **2000**, *52*, 241–260.
- (24) Mertes, S.; Lehmann, K.; Nowak, A.; Massling, A.; Wiedensohler, A. Link between aerosol hygroscopic growth and droplet activation observed for hill-capped clouds at connected flow conditions during FEBUKO. *Atmos. Environ.* **2005**, *39* (23–24), 4247–4256.
- (25) Mertes, S.; Galgon, D.; Schwirn, K.; Nowak, A.; Lehmann, K.; Massling, A.; Wiedensohler, A.; Wieprecht, W. Evolution of particle concentration and size distribution observed upwind, inside and downwind hill cap clouds at connected flow conditions during FEBUKO. *Atmos. Environ.* **2005**, *39* (23–24), 4233–4245.
- (26) Sorooshian, A.; Corral, A. F.; Braun, R. A.; Cairns, B.; Crosbie, E.; Ferrare, R.; Hair, J.; Kleb, M. M.; Mardi, A. H.; Maring, H.; et al. Atmospheric Research Over the Western North Atlantic Ocean Region and North American East Coast: A Review of Past Work and Challenges Ahead. J. Geophys. Res.: Atmos. 2020, 125 (6), No. e2019ID031626.
- (27) Corral, A. F.; Braun, R. A.; Cairns, B.; Gorooh, V. A.; Liu, H.; Ma, L.; Mardi, A. H.; Painemal, D.; Stamnes, S.; van Diedenhoven, B.; et al. An Overview of Atmospheric Features Over the Western North Atlantic Ocean and North American East Coast Part 1: Analysis of Aerosols, Gases, and Wet Deposition Chemistry. *J. Geophys. Res.: Atmos.* **2021**, *126* (4), No. e2020JD032592.
- (28) Painemal, D.; Corral, A. F.; Sorooshian, A.; Brunke, M. A.; Chellappan, S.; Gorooh, V. A.; Ham, S.-H.; O'Neill, L.; Smith, W. L. Jr.; Tselioudis, G.; et al. An Overview of Atmospheric Features Over the Western North Atlantic Ocean and North American East Coast Part 2: Circulation, Boundary Layer, and Clouds. *J. Geophys. Res.: Atmos.* 2021, 126 (6), No. e2020JD033423.
- (29) Sorooshian, A.; Alexandrov, M. D.; Bell, A. D.; Bennett, R.; Betito, G.; Burton, S. P.; Buzanowicz, M. E.; Cairns, B.; Chemyakin, E. V.; Chen, G.; et al. Spatially coordinated airborne data and complementary products for aerosol, gas, cloud, and meteorological studies: the NASA ACTIVATE dataset. *Earth Syst. Sci. Data* **2023**, *15* (8), 3419–3472.
- (30) Sorooshian, A.; Anderson, B.; Bauer, S. E.; Braun, R. A.; Cairns, B.; Crosbie, E.; Dadashazar, H.; Diskin, G.; Ferrare, R.; Flagan, R. C.; et al. Aerosol-Cloud-Meteorology Interaction Airborne Field Investigations: Using Lessons Learned from the U.S. West Coast in the Design of ACTIVATE off the U.S. East Coast. *Bull. Am. Meteorol. Soc.* **2019**, *100* (8), 1511–1528.
- (31) McNaughton, C. S.; Clarke, A. D.; Howell, S. G.; Pinkerton, M.; Anderson, B.; Thornhill, L.; Hudgins, C.; Winstead, E.; Dibb, J. E.; Scheuer, E.; et al. Results from the DC-8 Inlet Characterization Experiment (DICE): Airborne Versus Surface Sampling of Mineral Dust and Sea Salt Aerosols. *Aerosol Sci. Technol.* **2007**, *41* (2), 136–159.
- (32) Shingler, T.; Dey, S.; Sorooshian, A.; Brechtel, F. J.; Wang, Z.; Metcalf, A.; Coggon, M.; Mülmenstädt, J.; Russell, L. M.; Jonsson, H. H.; et al. Characterisation and airborne deployment of a new counterflow virtual impactor inlet. *Atmos. Meas. Technol.* **2012**, *5* (6), 1259–1269.

- (33) Shingler, T.; Crosbie, E.; Ortega, A.; Shiraiwa, M.; Zuend, A.; Beyersdorf, A.; Ziemba, L.; Anderson, B.; Thornhill, L.; Perring, A. E.; et al. Airborne characterization of subsaturated aerosol hygroscopicity and dry refractive index from the surface to 6.5 km during the SEAC4RS campaign. *J. Geophys. Res. Atmos.* **2016**, *121* (8), 4188–4210.
- (34) Moore, R. H.; Wiggins, E. B.; Ahern, A. T.; Zimmerman, S.; Montgomery, L.; Campuzano Jost, P.; Robinson, C. E.; Ziemba, L. D.; Winstead, E. L.; Anderson, B. E.; et al. Sizing response of the Ultra-High Sensitivity Aerosol Spectrometer (UHSAS) and Laser Aerosol Spectrometer (LAS) to changes in submicron aerosol composition and refractive index. *Atmos. Meas. Technol.* 2021, 14 (6), 4517–4542.
- (35) Murphy, D. M.; Froyd, K. D.; Bourgeois, I.; Brock, C. A.; Kupc, A.; Peischl, J.; Schill, G. P.; Thompson, C. R.; Williamson, C. J.; Yu, P. Radiative and chemical implications of the size and composition of aerosol particles in the existing or modified global stratosphere. *Atmos. Chem. Phys.* **2021**, *21* (11), 8915–8932.
- (36) DeCarlo, P. F.; Dunlea, E. J.; Kimmel, J. R.; Aiken, A. C.; Sueper, D.; Crounse, J.; Wennberg, P. O.; Emmons, L.; Shinozuka, Y.; Clarke, A.; et al. Fast airborne aerosol size and chemistry measurements above Mexico City and Central Mexico during the MILAGRO campaign. *Atmos. Chem. Phys.* **2008**, *8*, 4027–4048.
- (37) Zhang, Q.; Alfarra, M. R.; Worsnop, D. R.; Allan, J. D.; Coe, H.; Canagaratna, M. R.; Jimenez, J. L. Deconvolution and Quantification of Hydrocarbon-like and Oxygenated Organic Aerosols Based on Aerosol Mass Spectrometry. *Environ. Sci. Technol.* **2005**, *39*, 4938–4952.
- (38) Crosbie, E.; Shook, M. A.; Ziemba, L. D.; Anderson, B. E.; Braun, R. A.; Brown, M. D.; Jordan, C. E.; MacDonald, A. B.; Moore, R. H.; Nowak, J. B.; et al. Coupling an online ion conductivity measurement with the particle-into-liquid sampler: Evaluation and modeling using laboratory and field aerosol data. *Aerosol Sci. Technol.* **2020**, 54 (12), 1542–1555.
- (39) Kirschler, S.; Voigt, C.; Anderson, B.; Campos Braga, R.; Chen, G.; Corral, A. F.; Crosbie, E.; Dadashazar, H.; Ferrare, R. A.; Hahn, V.; et al. Seasonal updraft speeds change cloud droplet number concentrations in low-level clouds over the western North Atlantic. *Atmos. Chem. Phys.* **2022**, 22 (12), 8299–8319.
- (40) Kirschler, S.; Voigt, C.; Anderson, B. E.; Chen, G.; Crosbie, E. C.; Ferrare, R. A.; Hahn, V.; Hair, J. W.; Kaufmann, S.; Moore, R. H.; et al. Overview and statistical analysis of boundary layer clouds and precipitation over the western North Atlantic Ocean. *Atmos. Chem. Phys.* **2023**, 23 (18), 10731–10750.
- (41) Korolev, A.; Milbrandt, J. How Are Mixed-Phase Clouds Mixed? *Geophys. Res. Lett.* **2022**, 49 (18), No. e2022GL099578.
- (42) Xiao, Q.; Zhang, J.; Wang, Y.; Ziemba, L. D.; Crosbie, E.; Winstead, E. L.; Robinson, C. E.; DiGangi, J. P.; Diskin, G. S.; Reid, J. S.; et al. New particle formation in the tropical free troposphere during CAMP2Ex: statistics and impact of emission sources, convective activity, and synoptic conditions. *Atmos. Chem. Phys.* **2023**, 23 (17), 9853–9871.
- (43) Hair, J. W.; Hostetler, C. A.; Cook, A. L.; Harper, D. B.; Ferrare, R. A.; Mack, T. L.; Welch, W.; Izquierdo, L. R.; Hovis, F. E. Airborne High Spectral Resolution Lidar for profiling aerosol optical properties. *Appl. Opt.* **2008**, *47*, 6734–6752.
- (44) Burton, S. P.; Ferrare, R. A.; Hostetler, C. A.; Hair, J. W.; Rogers, R. R.; Obland, M. D.; Butler, C. F.; Cook, A. L.; Harper, D. B.; Froyd, K. D. Aerosol classification using airborne High Spectral Resolution Lidar measurements methodology and examples. *Atmos. Meas. Technol.* **2012**, *5* (1), 73–98.
- (45) Schlosser, J. S.; Bennett, R.; Cairns, B.; Chen, G.; Collister, B. L.; Hair, J. W.; Jones, M.; Shook, M. A.; Sorooshian, A.; Thornhill, K. L.; et al. Maximizing the Volume of Collocated Data from Two Coordinated Suborbital Platforms. *J. Atmos. Ocean. Technol.* **2024**, *41* (2), 189–201.
- (46) Schlosser, J. S.; Stamnes, S.; Burton, S. P.; Cairns, B.; Crosbie, E.; Van Diedenhoven, B.; Diskin, G.; Dmitrovic, S.; Ferrare, R.; Hair, J. W.; et al. Polarimeter + Lidar-Derived Aerosol Particle Number Concentration. *Front. Remote Sens.* **2022**, 3, No. 885332.
- (47) Dadashazar, H.; Painemal, D.; Alipanah, M.; Brunke, M.; Chellappan, S.; Corral, A. F.; Crosbie, E.; Kirschler, S.; Liu, H.; Moore,

- R. H.; et al. Cloud drop number concentrations over the western North Atlantic Ocean: seasonal cycle, aerosol interrelationships, and other influential factors. *Atmos. Chem. Phys.* **2021**, *21* (13), 10499–10526.
- (48) Crosbie, E.; Ziemba, L. D.; Shook, M. A.; Shingler, T.; Hair, J. W.; Sorooshian, A.; Ferrare, R. A.; Cairns, B.; Choi, Y.; DiGangi, J.; et al. Measurement report: Cloud and environmental properties associated with aggregated shallow marine cumulus and cumulus congestus. *Atmos. Chem. Phys.* **2024**, *24* (10), 6123–6152.
- (49) Hoffmann, F.; Feingold, G. A Note on Aerosol Processing by Droplet Collision-Coalescence. *Geophys. Res. Lett.* **2023**, *50* (11), No. e2023GL103716.
- (50) Hegg, D. A.; Hobbs, P. V. The homogeneous oxidation of sulfur dioxide in cloud droplets. *Atmos. Environ.* **1979**, *13*, 981–987.
- (51) Edwards, E.-L.; Choi, Y.; Crosbie, E. C.; DiGangi, J. P.; Diskin, G. S.; Robinson, C. E.; Shook, M. A.; Winstead, E. L.; Ziemba, L. D.; Sorooshian, A. Sea salt reactivity over the northwest Atlantic: an indepth look using the airborne ACTIVATE dataset. *Atmos. Chem. Phys.* **2024**, 24 (5), 3349–3378.
- (52) Liu, H.; Zhang, B.; Moore, R. H.; Ziemba, L. D.; Ferrare, R. A.; Choi, H.; Sorooshian, A.; Painemal, D.; Wang, H.; Shook, M. A.; et al. Tropospheric aerosols over the western North Atlantic Ocean during the winter and summer deployments of ACTIVATE 2020: life cycle, transport, and distribution. *Atmos. Chem. Phys.* 2025, 25 (4), 2087–2121.
- (53) De Bock, L. A.; Joos, P. E.; Noone, K. J.; Pockalny, R. A.; Van Grieken, R. E. Single particle analysis of aerosols, observed in the marineboundary layer during the Monterey Area Ship Tracks Experiment (MAST), with respect to cloud droplet formation. *J. Atmos. Chem.* **2000**, *37*, 299–329.
- (54) Öström, E.; Noone, K. J.; Pockalny, R. A. Cloud Droplet Residual Particle Microphysics in Marine Stratocumulus Clouds Observed during the Monterey Area Ship Track Experiment. *J. Atmos. Sci.* **2000**, *57*, 2671–2683.
- (55) Hoppel, W. A.; Frick, G. M.; Larson, R. E. Effect of nonprecipitating clouds on the aerosol size distribution in the marine boundary layer. *Geophys. Res. Lett.* **1986**, *13*, 125–128.
- (56) Soloff, C.; Ajayi, T.; Choi, Y.; Crosbie, E. C.; DiGangi, J. P.; Diskin, G. S.; Fenn, M. A.; Ferrare, R. A.; Gallo, F.; Hair, J. W.; et al. Bridging gas and aerosol properties between the northeastern US and Bermuda: analysis of eight transit flights. *Atmos. Chem. Phys.* **2024**, 24 (18), 10385–10408.
- (57) Ajayi, T.; Choi, Y.; Crosbie, E. C.; DiGangi, J. P.; Diskin, G. S.; Fenn, M. A.; Ferrare, R. A.; Hair, J. W.; Hilario, M. R. A.; Hostetler, C. A.; et al. Vertical variability of aerosol properties and trace gases over a remote marine region: a case study over Bermuda. *Atmos. Chem. Phys.* **2024**, 24 (16), 9197–9218.
- (58) Karlsson, L.; Baccarini, A.; Duplessis, P.; Baumgardner, D.; Brooks, I. M.; Chang, R. Y.; Dada, L.; Dallenbach, K. R.; Heikkinen, L.; Krejci, R.; et al. Physical and Chemical Properties of Cloud Droplet Residuals and Aerosol Particles During the Arctic Ocean 2018 Expedition. J. Geophys. Res.: Atmos. 2022, 127 (11), No. e2021JD036383.
- (59) Hilario, M. R. A.; Crosbie, E.; Banaga, P. A.; Betito, G.; Braun, R. A.; Cambaliza, M. O.; Corral, A. F.; Cruz, M. T.; Dibb, J. E.; Lorenzo, G. R.; et al. Particulate Oxalate-To-Sulfate Ratio as an Aqueous Processing Marker: Similarity Across Field Campaigns and Limitations. *Geophys. Res. Lett.* **2021**, *48* (23), No. e2021GL096520.
- (60) Ervens, B.; Turpin, B. J.; Weber, R. J. Secondary organic aerosol formation in cloud droplets and aqueous particles (aqSOA): a review of laboratory, field and model studies. *Atmos. Chem. Phys.* **2011**, *11* (21), 11069–11102.
- (61) Blando, J. D.; Ervens, B. J. Secondary organic aerosol formation in cloud and fog droplets a literature evaluation of plausibility. *Atmos. Environ.* **2000**, 34, 1623–1632.
- (62) Targino, A. C.; Noone, K. J.; Drewnick, F.; Schneider, J.; Krejci, R.; Olivares, G.; Hings, S.; Borrmann, S. Microphysical and chemical characteristics of cloud droplet residuals and interstitial particles in continental stratocumulus clouds. *Atmos. Res.* **2007**, *86* (3–4), 225–240.

- (63) Ghan, S. J.; Schwartz, S. E. Aerosol properties and processes A path from field and laboratory measurements to global climate models. *Bull. Am. Meteorol. Soc.* **2007**, *88*, 1059–1083.
- (64) Anttila, T.; Vaattovaara, P.; Komppula, M.; Hyÿarinen, A.-P.; Lihavainen, H.; Kerminen, V.-M.; Laaksonen, A. Size-dependent activation of aerosols into cloud droplets at a subarctic background site during the second Pallas Cloud Experiment (2nd PaCE): method development and data evaluation. *Atmos. Chem. Phys.* **2009**, *9*, 4841–4854.
- (65) Shrivastava, M.; Berg, L. K.; Fast, J. D.; Easter, R. C.; Laskin, A.; Chapman, E. G.; Gustafson, W. I.; Liu, Y.; Berkowitz, C. M. Modeling aerosols and their interactions with shallow cumuli during the 2007 CHAPS field study. *J. Geophys. Res. Atmos.* 2013, 118 (3), 1343–1360.
- (66) Berg, L. K.; Shrivastava, M.; Easter, R. C.; Fast, J. D.; Chapman, E. G.; Liu, Y.; Ferrare, R. A. A new WRF-Chem treatment for studying regional-scale impacts of cloud processes on aerosol and trace gases in parameterized cumuli. *Geosci. Model Dev.* **2015**, *8* (2), 409–429.
- (67) Lee, H.-H.; Zheng, X.; Qiu, S.; Wang, Y. Numerical case study of the aerosol—cloud interactions in warm boundary layer clouds over the eastern North Atlantic with an interactive chemistry module. *Atmos. Chem. Phys.* **2025**, 25 (12), 6069–6091.
- (68) Drewnick, F.; Diesch, J. M.; Faber, P.; Borrmann, S. Aerosol mass spectrometry: particle—vaporizer interactions and their consequences for the measurements. *Atmos. Meas. Technol.* **2015**, *8* (9), 3811–3830.
- (69) Koenig, T. K.; Baidar, S.; Campuzano-Jost, P.; Cuevas, C. A.; Dix, B.; Fernandez, R. P.; Guo, H.; Hall, S. R.; Kinnison, D.; Nault, B. A.; et al. Quantitative detection of iodine in the stratosphere. *Proc. Natl. Acad. Sci. U. S. A.* 2020, 117 (4), 1860–1866.
- (70) Ovadnevaite, J.; Ceburnis, D.; Canagaratna, M.; Berresheim, H.; Bialek, J.; Martucci, G.; Worsnop, D. R.; O'Dowd, C. On the effect of wind speed on submicron sea salt mass concentrations and source fluxes. *J. Geophys. Res.: Atmos.* **2012**, *117* (D16), D16201.
- (71) Zorn, S. R.; Drewnick, F.; Schott, M.; Hoffmann, T.; Borrmann, S. Characterization of the South Atlantic marine boundary layer aerosol using an aerodyne aerosol mass spectrometer. *Atmos. Chem. Phys.* **2008**, *8*, 4711–4728.
- (72) Schill, G. P.; Froyd, K. D.; Murphy, D. M.; Williamson, C. J.; Brock, C. A.; Sherwen, T.; Evans, M. J.; Ray, E. A.; Apel, E. C.; Hornbrook, R. S.; et al. Widespread trace bromine and iodine in remote tropospheric non-sea-salt aerosols. *Atmos. Chem. Phys.* **2025**, 25 (1), 45–71.
- (73) Zhang, J.; Ninneman, M.; Joseph, E.; Schwab, M. J.; Shrestha, B.; Schwab, J. J. Mobile Laboratory Measurements of High Surface Ozone Levels and Spatial Heterogeneity During LISTOS 2018: Evidence for Sea Breeze Influence. *J. Geophys. Res.: Atmos.* 2020, 125 (11), No. e2019JD031961.
- (74) Fossum, K. N.; Ovadnevaite, J.; Ceburnis, D.; Preißler, J.; Snider, J. R.; Huang, R.-J.; Zuend, A.; O'Dowd, C. Sea-spray regulates sulfate cloud droplet activation over oceans. *npj Clim. Atmos. Sci.* **2020**, 3 (1), 14.
- (75) Ghan, S. J.; Guzman, G.; Abdul-Razzak, H. Competition between Sea Salt and Sulfate Particles as Cloud Condensation Nuclei. *J. Atmos. Sci.* **1998**, *55*, 3340–3347.
- (76) Siu, L. W.; Schlosser, J. S.; Painemal, D.; Cairns, B.; Fenn, M. A.; Ferrare, R. A.; Hair, J. W.; Hostetler, C. A.; Li, L.; Kleb, M. M.; et al. Retrievals of aerosol optical depth over the western North Atlantic Ocean during ACTIVATE. *Atmos. Meas. Technol.* **2024**, *17* (9), 2739–2759.
- (77) Kandler, K.; Schneiders, K.; Ebert, M.; Hartmann, M.; Weinbruch, S.; Prass, M.; Pöhlker, C. Composition and mixing state of atmospheric aerosols determined by electron microscopy: method development and application to aged Saharan dust deposition in the Caribbean boundary layer. *Atmos. Chem. Phys.* **2018**, *18* (18), 13429–13455.
- (78) Denjean, C.; Caquineau, S.; Desboeufs, K.; Laurent, B.; Maille, M.; Quiñones Rosado, M.; Vallejo, P.; Mayol-Bracero, O. L.; Formenti, P. Long-range transport across the Atlantic in summertime does not enhance the hygroscopicity of African mineral dust. *Geophys. Res. Lett.* **2015**, 42 (18), 7835–7843.

- (79) Bègue, N.; Tulet, P.; Pelon, J.; Aouizerats, B.; Berger, A.; Schwarzenboeck, A. Aerosol processing and CCN formation of an intense Saharan dust plume during the EUCAARI 2008 campaign. *Atmos. Chem. Phys.* **2015**, *15* (6), 3497–3516.
- (80) Sullivan, R. C.; Moore, M. J. K.; Petters, M. D.; Kreidenweis, S. M.; Roberts, G. C.; Prather, K. A. Effect of chemical mixing state on the hygroscopicity and cloud nucleation properties of calcium mineral dust particles. *Atmos. Chem. Phys.* **2009**, *9*, 3303–3316.
- (81) Kumar, P.; Sokolik, I. N.; Nenes, A. Measurements of cloud condensation nuclei activity and droplet activation kinetics of fresh unprocessed regional dust samples and minerals. *Atmos. Chem. Phys.* **2011**, *11* (7), 3527–3541.
- (82) Weinzierl, B.; Ansmann, A.; Prospero, J. M.; Althausen, D.; Benker, N.; Chouza, F.; Dollner, M.; Farrell, D.; Fomba, W. K.; Freudenthaler, V.; et al. The Saharan Aerosol Long-Range Transport and Aerosol—Cloud-Interaction Experiment: Overview and Selected Highlights. *Bull. Am. Meteorol. Soc.* **2017**, 98 (7), 1427–1451.
- (83) Edwards, E. L.; Corral, A. F.; Dadashazar, H.; Barkley, A. E.; Gaston, C. J.; Zuidema, P.; Sorooshian, A. Impact of various air mass types on cloud condensation nuclei concentrations along coastal southeast Florida. *Atmos. Environ.* **2021**, 254, No. 118371.

